The two-group model for noble metals: low-field Hall effect and DMR in the limit of high dislocation densities



1995 J. Phys.: Condens. Matter 7 3913

(http://iopscience.iop.org/0953-8984/7/20/011)

J. Phys.: Condens. Matter 7 (1995) 3913–3928. Printed in the UK

# The two-group model for noble metals: low-field Hall effect and DMR in the limit of high dislocation densities

F Sachslehner

Institut für Festkörperphysik der Universität Wien, Strudlhofgasse 4, A–1090 Wien, Austria

Received 22 February 1995, in final form 24 March 1995

**Abstract.** Low-field Hall effect (LFHE) data obtained at 4.2 K, and data on the deviations from Matthiessen's rule (DMR) obtained between 4.2–140 K, of dislocated high-purity silver, gold and copper are compared in order to complete and extend a previous investigation of copper. The corrections to the two-group model (TGM) necessary to bring the anisotropy parameters for electron–dislocation scattering obtained from LFHE and DMR into coincidence are discussed in terms of the different Fermi surfaces and Fermi velocities as well as relaxation-time distributions. New insight is gained into the fact that these corrections are moderate, although the assumptions of the TGM are rather far from being fulfilled. The systematic changes of the anisotropy parameters estimated from the corrected TGM (0.09 for Ag, 0.11 for Cu and 0.13 for Au) are in qualitative agreement with the Watts model of electron–dislocation scattering.

## 1. Introduction

The purpose of this paper is to extend systematically a recent investigation on the low-field Hall effect (LFHE) and deviations from the Matthiessen rule (DMR) of dislocated copper [1] to high-purity silver and gold. First, there does not exist a common view of the two-group model (TGM) in all three noble metals. Second, there is increased interest in the context of electron–dislocation scattering from both the theoretical [2, 3] and practical [4] points of view. As in [1], we perform the present investigation in the limit of high dislocation densities and in very pure metals. We emphasize that measurements and calculations of LFHE and DMR will provide a critical test of the TGM. The present Fermi surface integrals have an accuracy that has never before been published. In particular, systematic comparisons of the results for all three noble metals could clarify the importance of the TGM correction and confirm the results obtained on copper alone. Using a DC-SQUID picovoltmeter [5] we have measured the Hall coefficient at 4.2 K in the true low-field condition.

Calculations of the low-field Hall coefficient ($R_H$) within the TGM have been done until recently only for silver and copper [6], and then not with the accuracy available today. Therefore, particularly in the case of silver, the interpretation of earlier LFHE data [7] and DMR data [8] based on [6] has been subject to large errors. Later, Barnard [9] estimated the Fermi surface integrals for copper (by fitting to formulae, in contrast to integrals calculated from known Fermi surfaces) for the calculation of $R_H$ using a mixture of de Haas–van Alphen results [10], DMR and LFHE data on dislocated copper. These values of the Fermi surface integrals with rather limited accuracy [1] were applied by several authors [11–16] in order to estimate the anisotropic scattering of conduction electrons from experimental values of $R_H$ for different samples of copper and copper alloys. For the determination of scattering anisotropy an accurate knowledge of experimental and theoretical values of $R_H$

0953-8984/95/203913+16$19.50  

is in general very important. For high-purity gold there has existed, up until now, neither a true low-field measurement of $R_H$ at 4.2 K nor a calculation within the TGM.

The TGM, in the form of a two-scatterer formula [17], was frequently used for discussing with reasonable success the qualitative behaviour of DMR data in noble metals as being due to phonons and impurities [17–19] or phonons and dislocations [8, 20]. However, only rough estimates [10, 17] or fits [19] of the TGM parameters were used. All the DMR calculations in this paper are done routinely with a three-scatterer formula [21]. In addition, it is shown that the DMR formulae in general need a correction term; however, this term seems to be negligible for our application.

## 2. The models

Our comparison of LFHE and DMR will be based on an exact expression of $R_H$ written as a corrected TGM (see [1]):

$$-R_H = sf[1 + (r/s)A_j^2 a]/(1 + A_j b)^2 \tag{1}$$

where

$$A_j = \tau_{Nj}/\tau_{Bj} \qquad f = \frac{12\pi^3}{e}\frac{\int_B v^2(k)\kappa(k)\,dS}{\left[\int_B v(k)\,dS\right]^2}$$

$$\tau_{Nj} = \frac{\int_N v(k)\tau_j(k)\,dS}{\int_N v(k)\,dS} \qquad \tau_{Bj} = \frac{\int_B v(k)\tau_j(k)\,dS}{\int_B v(k)\,dS}$$

$$r = \frac{\int_N v^2(k)\tau_j^2(k)\kappa(k)\,dS}{(\tau_{Nj})^2\int_N v^2(k)\kappa(k)\,dS} \qquad s = \frac{\int_B v^2(k)\tau_j^2(k)\kappa(k)\,dS}{(\tau_{Bj})^2\int_B v^2(k)\kappa(k)\,dS}$$

$$a = \frac{\int_N v^2(k)\kappa(k)\,dS}{\int_B v^2(k)\kappa(k)\,dS} \qquad b = \frac{\int_N v(k)\,dS}{\int_B v(k)\,dS}.$$

If the corrections are omitted, i.e. $r = s = 1$, equation (1) reduces to

$$-R_H = f(1 + A_j^2 a)/(1 + A_j b)^2 \tag{2}$$

where $A_j$ is the anisotropy parameter of scatterer $j$, $v$ is the Fermi velocity, $\tau_j$ is the relaxation time due to the scatterer $j$, and $k$ is the mean curvature on the Fermi surface.

Well defined anisotropy parameters can be calculated from (1) and (2) only if $R_H$ is measured in each case for one dominant scatterer. Below we will need $A_{ph}$, $A_{im}$ and $A_{dis}$, the anisotropy parameters for phonon, impurity and dislocation scattering respectively. In principle, these values can be obtained from the Hall coefficients of annealed undeformed samples at room temperature ($R_H^{300}$(ph)) and at 4.2 K ($R_H^{4.2}$(im)) and sufficiently dislocated samples at 4.2 K ($R_H^{4.2}$(dis)).

For the calculation of the DMR ($\delta$) (intending a concrete interpretation only at 130 K) we use the formula of Dugdale and Basinski [17] extended to three scatterers [21]:

$$\delta = \sum_{j=1}^{3} \rho_j \rho_{j+1} b A_{j+2}(A_j - A_{j+1})^2 \left(\sum_{j=1}^{3} \rho_j (1 + bA_j)^2 A_{j+1} A_{j+2}\right)^{-1} \tag{3}$$

in the cyclic notation $\rho_4 = \rho_1$, $\rho_5 = \rho_2$, $A_4 = A_1$, $A_5 = A_2$, where $A_j$ is the scattering anisotropy parameter of the $j$th scatterer (phonons, impurities and dislocations) and $\rho_j$ is the resistivity of the $j$th scatterer on its own. The term $b$ is the same as in (1).

Agreement between DMR $\delta$ and $R_H$ is achieved when the $b$ and $A_j$ used in (3) are identical to the quantities in (1) or (2) for each scatterer $j$.

We emphasize that, in general, equation (3) gives the DMR as being somewhat too low. This is again due to the fact that the TGM does not specify the exact $k$-dependence of relaxation times, which would require for each point on the Fermi surface (three scatterers)

$$\frac{1}{\tau_{tot}(k)} = \left(\sum_{j=1}^{3} \frac{1}{\tau_j(k)}\right)^{-1} \tag{4}$$

where $\tau_{tot}(k)$ is the total relaxation time at the point $k$. As shown in appendix A, the additional DMR $\Delta\delta$ can be estimated as

$$\Delta\delta \approx u(\rho_1 + \rho_2 + \rho_3 + \delta) \qquad u > 0$$

with

$$u = 1 - \int_B \left(\sum_{j=1}^{3} \frac{1}{\tau_j(k)}\right)^{-1} v(k)\,dS \left[\left(\sum_{j=1}^{3} \frac{1}{\tau_{Bj}(k)}\right)^{-1} \int_B v(k)\,dS\right]^{-1}.$$

Since $\tau_{tot}(k)$ is a function of temperature the correction parameter $u$ will also depend on temperature. If we neglect the influence of impurities (the case of high-purity samples) the absolute correction will be highest for $\rho_{ph} \approx \rho_{dis}$ and will decrease in parallel with the DMR described by the TGM.

## 3. Experimental details

First, foils with a thickness of about 250 $\mu$m were prepared using various heat treatments and rolling procedures. We used the following techniques.

(i) MARZ silver (MRC): 99.99% pure silver slug (diameter 12 mm, length 11.8 mm); rolling (always in a stainless steel sandwich) to a thickness of 2.5 mm; annealing at 550 °C for 7 h; rolling to a thickness of 0.5 mm; annealing at 550 °C for 7 h; rolling to 250 $\mu$m; annealing at 800 °C for 10 h in high vacuum (obtained residual resistivity 10 n$\Omega$ cm) followed by 7 h oxygen annealing at 800 °C at a dynamic pressure of $1 \times 10^{-5}$ mbar [22]. Resulting residual resistivity: 2.3 n$\Omega$ cm.

(ii) Gold (ÖGUSSA): 99.99% pure gold sheet with $25 \times 0.5$ mm cross section; rolling (always in a stainless steel sandwich) to a thickness of about 250 $\mu$m; annealing at 600 °C for 10 h in high vacuum. The result was a residual resistivity of 11.5 n$\Omega$ cm. In order to get a lower value the gold sheets were annealed at 950 °C for 4 h in high vacuum followed by an oxygen anneal at 950 °C for 22 h under normal atmospheric air pressure [23]. The result was a residual resistivity of 2.3 n$\Omega$ cm.

The produced foils of silver and gold were cut into three pieces: in each case one piece remained as prepared in the undeformed (annealed) condition as a reference sample; dislocations were introduced into the second and third pieces by rolling to true strains, $\varepsilon$,

of about 50% and 100%, respectively (see table 3 in section 3.4). Vacancies were annealed out at room temperature.

The final samples were made by spark erosion as in [1]. Details of LFHE at 4.2 K, and DMR measurements between 4.2–140 K have already been described in [1]. DMR and LFHE measurements were always made on the same sample. We describe the DMR at temperature $T$ by the experimental dislocation resistivity

$$\rho_{d,ex}(T) = \rho(T, \varepsilon) - \rho(T, \varepsilon = 0)$$

where $\rho(T, \varepsilon)$ and $\rho(T, \varepsilon = 0)$ are the resistivities of the dislocated sample and the undeformed reference sample, respectively. From $\rho_{d,ex}(4.2\,K)$ we estimated the true dislocation resistivity $\rho_d$ (see [12]), which will be necessary for DMR calculations by equation (3), by taking into account the DMR between impurities and dislocations. Annealing of the deformed silver samples in order to find the geometry factors (using ideal resistivity data of the noble metals [24]) was performed in high vacuum at 550 °C for 7 h. A similar procedure for the gold samples was done under normal atmospheric air pressure at 600 °C for 10 h.

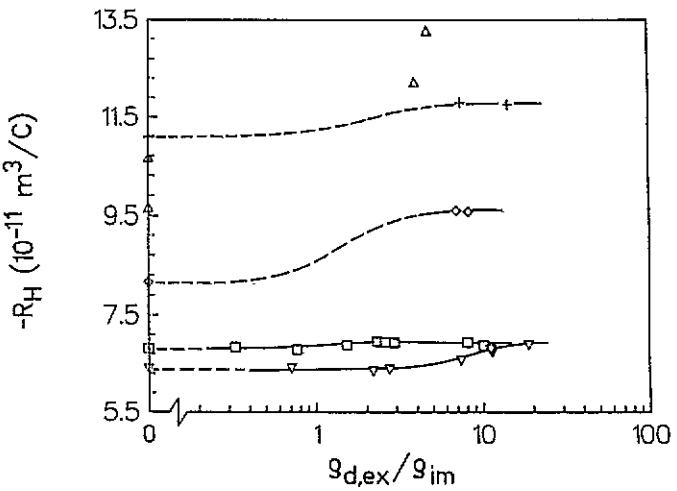


**Figure 1.** Hall coefficient, $R_H$, at 4.2 K as a function of the ratio of experimental dislocation resistivity to impurity resistivity, $\rho_{d,ex}/\rho_{im}$. +, silver; △, silver data after Barnard [7]; ◇, gold; □, ME copper and ▽, MRC copper after [1]. Broken curves: expected behaviour according to the results of copper.

## 4. Results and discussion

### *4.1. Hall effect*

Figure 1 shows the Hall coefficient $R_H$ at 4.2 K as a function of the ratio of dislocation resistivity $\rho_{d,ex}$ to impurity resistivity $\rho_{im}$ for the copper, gold and silver samples investigated. For comparison, the results on the MRC and ME copper of [1] are also presented. The relation of the undeformed gold and silver samples to the highly deformed samples is analogous to that of the copper samples. This is indicated by the broken curves drawn in

analogy to the results for copper, and can be explained as in [1]. As intended, the deformed gold and silver samples lie at a value $\rho_{d,ex}/\rho_{im} \sim 10$ and $R_H$ is independent of deformation within the error limits, as is the case for copper. We conclude that, in the samples with $\varepsilon$ near and above 50%, electron–dislocation scattering dominates and that the related Hall coefficients are a measure of the anisotropy of electron–dislocation scattering. A comparison with the silver data of Barnard [7] in figure 1 shows that results for the undeformed samples are roughly in agreement in the case of one sample; however Barnard's deformed samples lie slightly higher, having a ratio $\rho_{d,ex}/\rho_{im} \sim 4$–5. This could be due to Barnard's deformation method: he used bending.

**Table 1.** Hall coefficient in different states. (Units: $10^{-11}\,m^3\,C^{-1}$.)

| Condition | Cu | Ag | Au |
|---|---|---|---|
| $R_H^{300}$(ph), $\varepsilon = 0$ | −5.08 | −8.70 | −7.06 |
| $R_H^{4.2}$(im), $\varepsilon = 0$ | −6.38 to −6.82[a] | −11.09 | −8.16 |
| $R_H^{4.2}$(dis), $\varepsilon \approx 0.5$ | −6.90 | −11.80 | −9.61 |
| $R_H^{4.2}$(dis), $\varepsilon \approx 1$ | −6.89 | −11.76 | −9.59 |
| $R_H$(fe)[b] | −7.37 | −10.65 | −10.59 |

[a] See [1].
[b] $R_H$(fe) is the free-electron Hall coefficient.

In table 1 the most important $R_H$ values of figure 1 are summarized, and completed by our measured room-temperature data. The measured values of $R_H$ given in table 1 have a total error of ±1%; however the reproducibility of $R_H$ was about ±0.3%.

### *4.2. DMR*

The normalized DMR-data of silver, copper and gold for dislocations and phonons as main scatterers can be seen in figures 2–4 (points), where $D = \rho_{d,ex}(T)/\rho_{d,ex}(4.2)$. The data for copper are taken from [1]. The experimental data for all three noble metals are very similar, as expected. The points for the higher deformed samples are always lower than for the smaller deformations, in accordance with theory [2]. The total height of the experimental data at about 130 K (or the step height) decreases slightly from copper to silver to gold. The DMR-curves for gold increase more rapidly at lower temperatures than those of silver and copper. This behaviour is similar to the increase of the ideal phonon resistivity of the noble metals [24], and corresponds to the lower Debye temperature. The most interesting DMR-data are summarized in table 2. The broken and full curves are discussed later.

### *4.3. The two-group model and corrections*

*4.3.1. The Fermi surface parameters.* One of the most important parameters of the TGM is the choice of a suitable neck angle. From the viewpoint of physics, the best choice for the boundary between neck and belly region can be found according to the shape of the Fermi surface (the intersection between the neck and the approximately spherical part of the belly which coincides in that region rather well with the free-electron sphere [28]) and the variation of relaxation times due to the difference of s- and d-like and p-like scatterers [25], respectively. In the approximation of the TGM the neck angle defines the neck region of the experimentally determined Fermi surface [26] to lie within a cone about the ⟨111⟩ direction. The terms $a$, $b$ and $f$ in (1) and (2), and $b$ in (3), will vary according to $\theta$. In order to overcome the somewhat mysterious choice of $\theta$ in the past, in figure 5 the variation of $a$, $b$

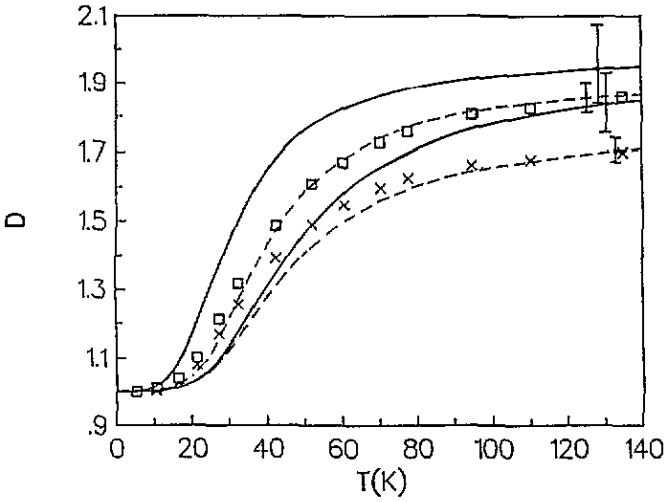


**Figure 2.** Normalized DMR-curves ($D = \rho_{d,ex}(T)/\rho_{d,ex}(4.2\,K)$) for silver samples as a function of temperature, $T$. Points: experiment; broken curves: fit calculations giving $A_{dis}$(DMR); full curve: DMR calculation using $A_{dis}$ (Hall) of table 3. Sample Ag50. □, experimental points; – – –, $A_{dis}$ (DMR) = 0.146 and $\rho_{dis}$ = 15.62 nΩ cm; ——, $A_{dis}$(Hall) = 0.139 and $\rho_{dis}$ = 15.61 nΩ cm. Sample Ag100: ×, experimental points; – – –, $A_{dis}$ (DMR) = 0.166 and $\rho_{dis}$ = 29.15 nΩ cm; ——, $A_{dis}$(Hall) = 0.144 and $\rho_{dis}$ = 29.11 nΩ cm.

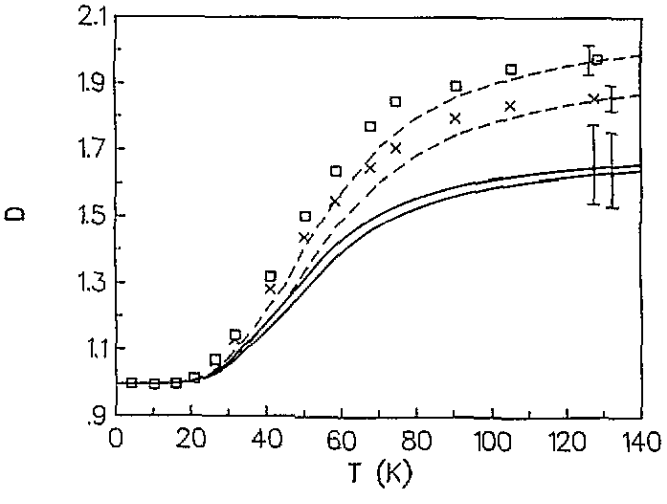


**Figure 3.** Normalized DMR-curves for copper (after [1]). The meaning of the curves is as in figure 2. Sample Cu50: □, experimental points; – – –, $A_{dis}$ (DMR) = 0.102 and $\rho_{dis}$ = 13.09 nΩ cm; ——, $A_{dis}$(Hall) = 0.144 and $\rho_{dis}$ = 13.11 nΩ cm. Sample Cu100: ×, experimental points; – – –, $A_{dis}$ (DMR) = 0.113 and $\rho_{dis}$ = 16.24 nΩ cm; ——, $A_{dis}$(Hall) = 0.147 and $\rho_{dis}$ = 16.25 nΩ cm.

and $f$ with $\theta$ is shown for all three noble metals as calculated by Watts [27] based on the precise Fermi surface data of Halse [26].

As it seems to be impractical to change the neck angle according to the detailed anisotropy of the dominant scattering mechanism, the *most general choice* is a set of $a$,

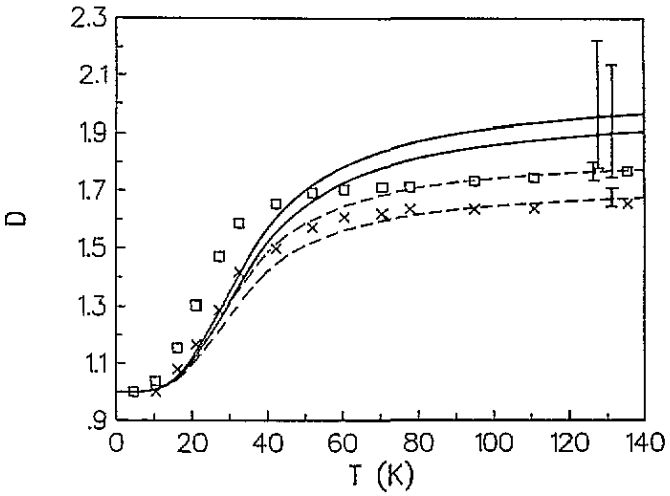


**Figure 4.** Normalized DMR-curves for gold. The meaning of curves is as in figure 2. Sample Au50: □, experimental points; – – –, $A_{dis}$ (DMR) = 0.125 and $\rho_{dis}$ = 15.15 nΩ cm; ——, $A_{dis}$(Hall) = 0.104 and $\rho_{dis}$ = 15.13 nΩ cm. Sample Au100: ×, experimental points; – – –, $A_{dis}$ (DMR) = 0.139 and $\rho_{dis}$ = 17.20 nΩ cm; ——, $A_{dis}$(Hall) = 0.109 and $\rho_{dis}$ = 17.18 nΩ cm.

$b$ and $f$ with $a = 0$, as described in [1]. With this choice the corrections connected with $r \neq 1$ are minimized on average (as different scattering anisotropies are concerned).

We can see in figure 5($a$) that the term $a$ reaches zero at a neck angle $\theta = 18.7°$ for copper, 17.9° for gold and 12.9° for silver (arrows in figure 5($a$)). In a comparison of these angles with the mean angles where the neck dives into the approximately spherical part of the belly or free-electron Fermi surface [28], the respective values for copper (18.5°) and gold (17.5°) nearly coincide, whereas for silver (16.5°) there is a strong discrepancy. This is due to the fact that the neck diameter at the Brillouin zone in silver is strongly reduced compared with copper and gold [28]. So the negative part of $\int_N v^2\kappa \, dS$ (the numerator of the term $a$) is balanced by a comparably smaller neck region (up to only 12.9°) with positive curvature shifting the $a$ value for silver in figure 5($a$) to the left so that it lies higher than the copper and gold curves. The fact that the value of 12.9° is so far from the physically indicated angle of 16.5° makes a comparison of the results difficult, because the anisotropy factors are not calculated from the corresponding regions and the TGM might fail if regions with strongly reduced curvature are counted as parts of the belly.

**Table 2.** DMR data of the samples used.

| Sample | $\varepsilon$ (%) | $\rho_{d,ex}$(4.2 K) | $\rho_{d,ex}$(77 K) | $D$(130 K) |
|---|---|---|---|---|
| Cu50 | 49 | 13.29 | 24.62 | 1.975 |
| Ag50 | 43 | 16.20 | 28.50 | 1.859 |
| Au50 | 66 | 15.50 | 26.52 | 1.768 |
| Cu100 | 82 | 16.34 | 28.10 | 1.855 |
| Ag100 | 116 | 26.70 | 48.30 | 1.699 |
| Au100 | 112 | 17.54 | 28.71 | 1.673 |

The $b$ curves (figure 5($b$)) nearly coincide for all three noble metals. This term does not show the differences so much because it depends only linearly on the Fermi velocity.

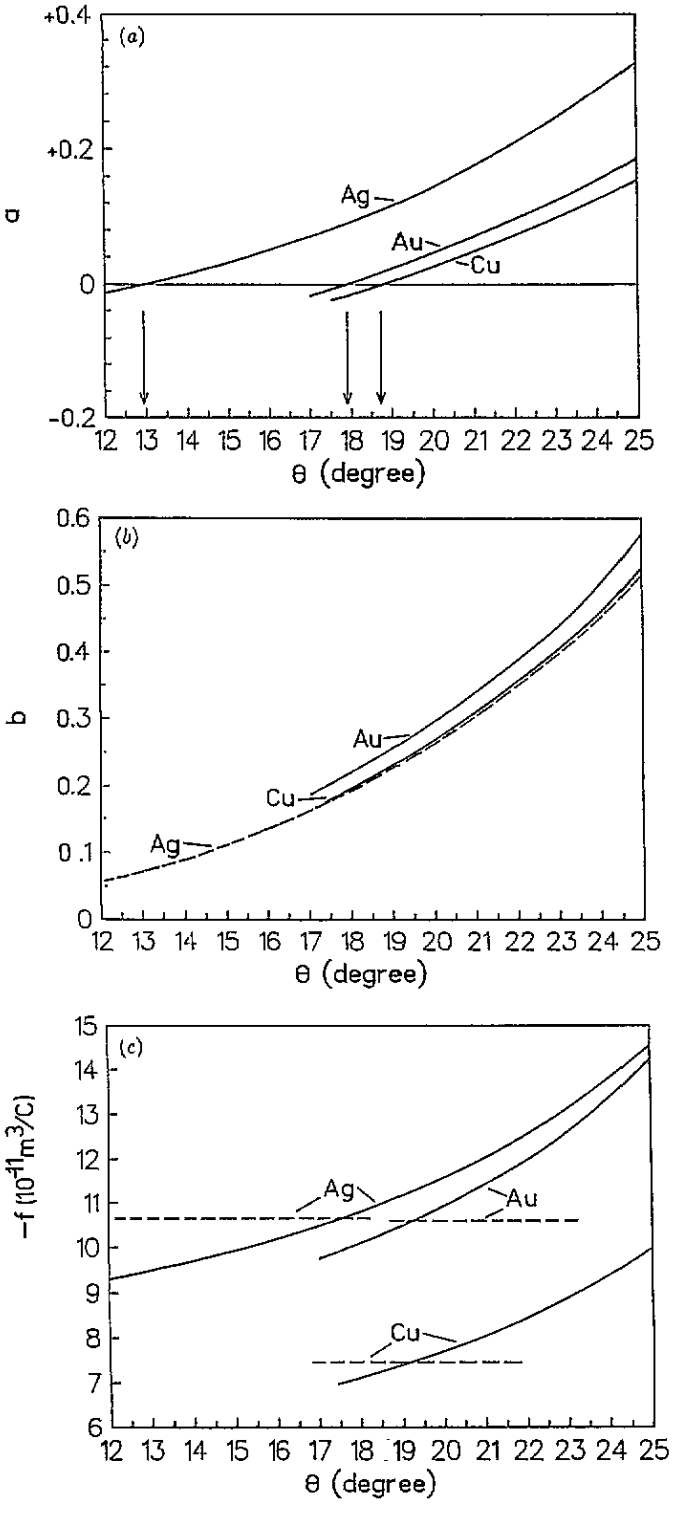


**Figure 5.** Fermi surface integral terms $a$, $b$ and $f$ as a function of neck angle $\theta$. (*a*) $a$ term; the arrows indicate the value of $\theta$ where $a = 0$. (*b*) $b$ term. (*c*) $f$ term; the broken curves indicate the free-electron Hall coefficients of the noble metals.

The term $f$ (figure 5(*c*)) is inversely proportional to the electron density and has the same dimension as $R_H$; $f$ is the leading term of equation (1). The remaining factor $(1 + A^2a)/(1 + bA)^2$ in (2) only diminishes the height of $R_H$ given by $f$ by several per cent in the case of electron–dislocation scattering, as can be proved easily by values of $A_{dis}$(Hall) of table 3 below.

For the $f$ curves shown the following lattice constants were used: Cu: 3.603 03 Å; Ag: 4.069 31 Å and Au: 4.065 06 Å [29]; (all values at 25 K). If (1) and (2) are used for room-temperature values of $R_H$, the $f$ term has to be increased by 1% due to thermal expansion. In this context it is of interest to compare $f$ with the free-electron Hall coefficient $R_H$(fe), which is done by the broken horizontal lines in figure 5(*c*). In the case of copper and gold the $f$ value of around 20° does not lie very much higher than $R_H^{4.2}$(dis) from table 1 (being lower than $R_H$(fe)). For silver, however, the $f$ curve indicates again that an angle of 12.9° cannot be used due to the large difference between $f$ and $R_H$(fe), but an angle $\theta$ near 16.5° seems to be more suitable for a correct description. Additionally, for silver, we have $R_H^{4.2}$(dis) > $R_H$(fe) (see table 1).

*4.3.2. Calculations of anisotropy parameters.* Figure 6 shows the effect on $A_{ph}$ and $A_{dis}$ calculated by (2) (usual TGM) from the values of $R_H^{300}$(ph) and $R_H^{4.2}$(dis) in table 1 if the terms $a$, $b$ and $f$ are varied with the neck angle as presented in figure 5. The curves for $A_{ph}$(300 K) of gold and copper almost coincide, show nearly no dependence on $\theta$ (being a rather good indication for isotropic scattering) and lie around the value 0.95, which is close to the isotropic value $A_{ph} = 1$. The value of $A_{ph}$ for silver lies considerably lower, and varies from 0.73 to 0.8. This is once more surprising because silver has a similar lattice constant to gold and has a Debye temperature between that of copper and gold; only its Fermi surface, with its smaller necks and smaller bulges deviates less from the free-electron sphere than that of copper and gold. The variation of $A_{ph}$ with $\theta$ could indicate some slight anisotropy of electron–phonon scattering at room temperature. The lower value for $A_{ph}$ of silver could stem from the incorrect averaging of relaxation times in the (usual) TGM. As will be shown in section 4.4 only a very small correction parameter ($s$) is needed to get isotropic electron–phonon scattering ($A_{ph} = 1$) for silver. In the past, the larger deviation from isotropic electron–phonon scattering in silver within the TGM was not found due to the large errors in the calculations and in the measurements of $R_H$ [6, 7, 30].

$A_{dis}$ values determined from $R_H$ are much more influenced by the choice of neck angle, as can be seen from the three lower curves in figure 6; $A_{dis}$ increases with increasing $\theta$. There is nearly no difference between copper and gold. Again, the curve for silver is shifted to obviously lower values of $A_{dis}$ due to the deviating neck proportion. In the conventional TGM the main point is that, for gold and copper, the $A_{dis}$ values for neck angles $\theta < 17°$ are negative while for silver that limit of the TGM is reached at $\theta < 21°$, although silver has the smallest necks of the noble metals. As a consequence the uncorrected TGM does not work for silver, neither with a physically motivated boundary angle of 16.5° nor at 12.9° as was expected.

Only formally can we try to find a suitable neck angle for silver yielding approximately the same $A_{dis}$ value as for the $a = 0$ version of copper and gold. We get $\theta = 23°$, which is 1° lower than the value suggested by Barnard [7]. Details of the calculation of anisotropy parameters (based on equation (2); conventional TGM) from $R_H^{4.2}$(dis) and $R_H^{300}$(ph) with the $a = 0$ version of copper and gold and the '$\theta = 23°$ version' of silver are summarized in table 3 (the obtained anisotropy parameters are marked as $A_{dis}$ (Hall) and $A_{ph}$ (Hall)). It can be seen that the values of $A_{dis}$ (Hall) due to the conventional TGM lie in the range 0.10–0.14. The Fermi surface parameters for the physically indicated neck angle of silver ($\theta = 16.5°$) are also shown in table 3.

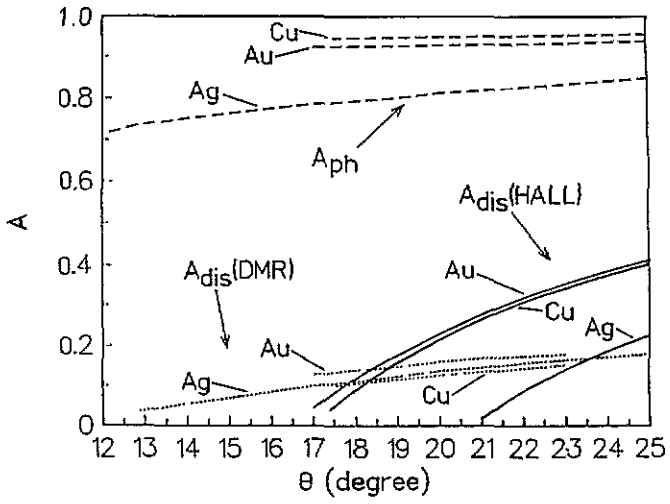


**Figure 6.** Variation of calculated anisotropy parameters $A$ with neck angle $\theta$. ——, $A_{dis}$ *calculated from* $R_H^{4.2}$ *(dis) by* (2); – – –, $A_{ph}$ *calculated from* $R_H^{300}$ *(ph) by* (2); · · · · · ·, $A_{dis}$ *(DMR)* calculated from the experimental DMR step height by (3).

**Table 3.** Model parameters: results of anisotropy parameters from Hall effect and DMR calculations. $f$, $a$ and $s$ are in units of $10^{-11}\,m^3\,C^{-1}$. A mean value of two samples is always given.

| | Cu | Ag | Au | Ag |
|---|---|---|---|---|
| $\theta$ | 18.7 | 23 | 17.9 | 16.5 |
| $a$ | 0 | 0.244 | 0 | 0.0613 |
| $b$ | 0.219 | 0.401 | 0.214 | 0.1501 |
| $f_{4.2\,K}$ | 7.343 | 13.095 | 10.046 | 10.339 |
| $f_{300\,K}$ | 7.417 | 13.260 | 10.147 | 10.470 |
| $A_{ph}$(Hall) | 0.949 | 0.836 | 0.927 | 0.782 |
| $A_{dis}$(Hall) | 0.145 | 0.141 | 0.107 | — |
| $A_{dis}$(DMR) | 0.107 | 0.156 | 0.132 | 0.0895 |
| $s_{dis}$ | 0.984 | 1.015 | 1.010 | 1.170 |
| $s_{ph}$ | 1.018 | 1.02[a] | 1.026 | 1.03[b] |

[a] $r = 1.101$ was used.
[b] $r = 1.127$ was used.

*4.3.3. DMR calculations.* In this section we attempt to describe the step height of DMR at 130 K ($D(130\,K) - 1$) in order to avoid the problem of the proper description of the anisotropy of electron–phonon scattering at lower temperatures, where violations of the relaxation-time approximation itself may occur [31]. In all cases we assume that the anisotropy of electron–phonon scattering is isotropic and does not change between 130–300 K. An attempt to explain quantitatively the DMR for $T < 130\,K$ must wait for new theoretical results.

For our DMR calculations we use (3) and the $b$ values of table 3. The connection of the DMR step height $D(130\,K) - 1$ with (3) is given by $D(T) = \delta(T)/[\rho_{d,ex}(4.2)] + 1$. In (3) we use the following values: $\rho_1 \equiv \rho_{ph}$, the ideal phonon resistivities [24]; $\rho_2 \equiv \rho_{im}$, the impurity resistivity at 4.2 K, which is 2.3 nΩ cm for our silver and gold samples; for copper see [1]; $\rho_3 \equiv \rho_{dis}$, the true dislocation resistivity which is about 0.2–0.5 nΩ cm lower than

$\rho_{d,ex}$ by taking into account the DMR due to $\rho_{im}$, $\rho_{dis}$, $A_{im}$ and $A_{dis}$; $A_{ph} = 1$, as stated in [1]; $A_{im} = 1$, since as in [1], due to the influence of grain boundaries, the values of $A_{im}$ obtained by LFHE seem to be too low; and $A_{dis}$, as shown in table 3 calculated from LFHE ($A_{dis}$ (Hall)) or as the only free parameter in order to fit the experimental step height at 130 K (given as $A_{dis}$ (DMR) in table 3).

Results of such calculations are shown in figures 2 (Ag, $\theta = 23°$), 3 (Cu, $\theta = 18.7°$), 4 (Au, $\theta = 17.9°$) and 7 ($\theta = 16.5°$) by the full curves ($A_{dis}$ (Hall)) and broken curves ($A_{dis}$ (DMR)). The broken curves are calculated under the condition that the experimental step height at 130 K is reproduced. Of course, the results for silver at $\theta = 23°$ (figure 2) may suffer from the unphysically large neck boundary angle. Comparing figures 2–4 we can see that a higher experimental curve always corresponds to a higher theoretical curve. In the case of gold (figure 4) the experimental step height is overestimated (as for silver) by the use of $A_{dis}$ (Hall), whereas for copper it is underestimated (figure 3). As shown in the next section, we can explain this behaviour if we take into account the different averaging procedures of relaxation times involved in LFHE and DMR, which are influenced by the different Fermi surface properties of each noble metal. The error bars for the full curves (only drawn for 130 K) are due to the experimental uncertainty of $A_{dis}$ (Hall) obtained from the total error (1%) of $R_H$ (dis). It must be noted that, compared with the total error, the scattering of the LFHE data is much smaller due to the high reproducibility (0.3%), as can be seen from the moderate differences between the values for the 50% and 100% deformed samples (see table 1). The fit calculations (broken curves) describe the experimental DMR curves (small error bars) at high temperatures quite well. Only for the samples Ag50 (figure 2) and Au50 (figure 4) is there some overlap of the error bars. This means we have the important result from figures 2–4 that the anisotropy parameters calculated from $R_H$ and DMR are different.

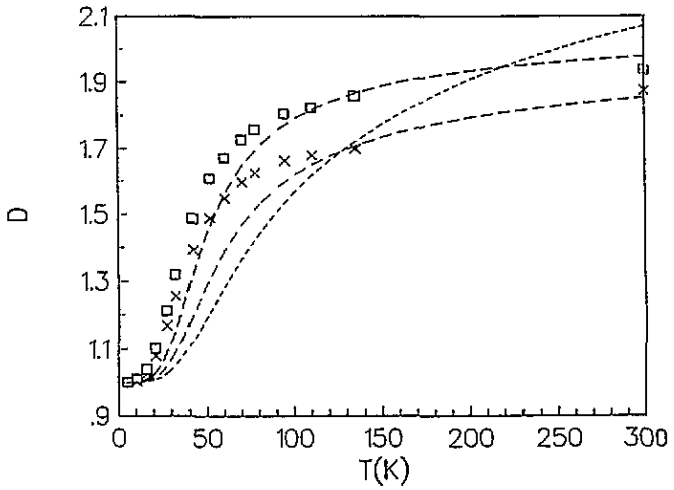


**Figure 7.** Normalized DMR-curves for the two deformed silver samples extended to room temperature. Points: experiment; long-dash broken curve: fit calculations with $\theta = 16.5°$. Sample Ag50: □, experimental points; – – –, $A_{dis}$ (DMR) = 0.086 and $\rho_{dis}$ = 15.92 nΩ cm. Sample Ag100: ×, experimental points; – – –, $A_{dis}$ (DMR) = 0.093 and $\rho_{dis}$ = 29.43 nΩ cm; – – –, $A_{dis}$ (DMR) = 0.036 and $\rho_{dis}$ = 29.56 nΩ cm with $\theta = 12.9°$.

Figure 7 shows that fits for the DMR step height of silver with a neck angle $\theta = 16.5°$ give reasonable results, particularly if the range of temperature is extended to room temperature.

However, the value of $A_{dis}$ (DMR) is drastically decreased compared to figure 2. As can be seen also in figure 7 the neck angle $\theta = 12.9°$ ($a = 0$ version) is not reasonable for silver. As summarized in table 3 (for simplicity the mean values of the two samples are given) we have from the DMR calculations with $A_{dis}$ (DMR) the important result that the anisotropy parameter for electron–dislocation scattering increases from silver (0.09; $\theta = 16.5°$) to copper (0.11) to gold (0.13). The same (qualitative) behaviour would be expected from the Watts model [32] of electron–dislocation scattering due to the fact that the bulges of the Fermi surface increase from silver to copper to gold. In contrast, in the case of silver the unphysically large neck angle $\theta = 23°$ falsifies the anisotropy parameter towards less anisotropy (0.15; see table 3). We note that the anisotropy parameter calculated from the usual TGM ($A_{dis}$ (Hall) in table 3) does not reflect the situation so clearly as $A_{dis}$(DMR) because of the more complicated averaging of the relaxation times (see the next section). However, we see in table 3 that both $A_{dis}$ (Hall) and $A_{dis}$ (DMR) lie in the rather limited range 0.08–0.15, showing some agreement between LFHE and DMR measurements.

The question arises: which range of neck angle should be taken into account in order to still get reasonable results. If we assume rather roughly that $0 < A_{dis} < 0.2$ the answer for the LFHE in the conventional TGM (see figure 6) is about $\pm 1°$. For the DMR we try to find it by fits of the experimental step height by varying the $b$ term with $\theta$. As a result, we get the variation of $A_{dis}$(DMR) with $\theta$ shown by the dotted curves in figure 6 (calculated only for the 100% deformed samples). It is obvious that the DMR fits require only a smooth variation of the anisotropy parameter $A_{dis}$ (DMR) with $\theta$. This means that, within the TGM, the DMR is better able to fix the principal magnitude of the anisotropy parameters than $R_H$. Otherwise, the LFHE is more suitable for the determination of the concrete neck angle. Formally, the experimental step height can always be fitted by (3) if $\theta$ is large enough (apart from the fact that the increase of the DMR curves may be unphysically steep). However, at too small angles even the step height cannot be described, as is shown in figure 7 for silver at $\theta = 12.9°$.

*4.3.4. Estimation of correction parameters.* As described by (1) the corrected TGM takes into account the different averaging of relaxation times for LFHE and electrical resistivity (DMR). The corrected TGM makes it possible that the same anisotropy parameters can be used for $R_H$ and DMR. Since the ratio $r/s$ is not known from experiment and is difficult to estimate, it seems to be useful (see section 4.3.1) to use (1) in the '$a = 0$ version', as was done successfully for Cu [1] and as will be shown below for the case of gold. So, using experimental values of $R_H$ and anisotropy parameters calculated from the DMR step height, $s$ values for different scatterers can be estimated using (1).

However, for all cases where the $a$ values are near zero the $a = 0$ version will be a rather good approximation (for all three noble metals). The accuracy of that approximation will depend on $A_j$. In the case of dominant electron–dislocation scattering ($A_{dis} \sim 0.1$, see table 3) we have the most favourable case, and can use an approximation with $a = 0$ for silver up to a neck angle of 23°. As can be estimated by the use of figure 5($a$), for silver such a calculation at $\theta = 23°$ underestimates $R_H$ (and $s$) by about 1%.

In fact, by applying our preferred neck angles (18.7° for copper and 17.9° for gold; $a = 0$ version; 23° for silver) and using the anisotropy parameters $A_{dis}$(DMR) of table 3, equation (1), using $R_H$(dis), gives $s$ values near unity ($s \approx 0.98$–$1.02$). The exception is for the physically indicated angle of silver ($\theta = 16.5°$) where a value $s \approx 1.17$ is needed ($a \approx 0$ approximation). The exact numbers, indicated as $s_{dis}$ (mean value of two samples), can be seen in table 3. Analogous to the DMR curves calculated by $A_{dis}$ (Hall) (see figures 2–4) $s_{dis}$ for copper is slightly lower than unity, whereas the values for gold and silver are larger than unity.

In a similar way we can calculate, from $R_H^{300}$(ph) of table 1, the required number $s$ for exactly isotropic electron–phonon scattering by using the neck angles from above. The results are indicated in table 3 as $s_{ph}$, and have values of about 1.02–1.03, where the highest correction is needed once more for the physically indicated neck angle of silver. However, to get this value for silver, some guess of the number $r$ was necessary. We used $r = 1.101$ ($\theta = 23°$) and $r = 1.127$ ($\theta = 16.5°$) assuming that the deviation of $r$ from unity should be somewhat larger than that of $s$ [1]. It can be seen in table 3 that the variation of $s_{ph}$ is not so significant as that of $s_{dis}$, therefore these values are not discussed further.

*4.3.5. The relation of correction parameters to the Fermi surface properties.* In this section we give an interpretation of the variation of the $s$ values for electron–dislocation scattering calculated above for the physically indicated neck angles ($s_{dis}$ in table 3). In order to discuss changes of $A_{dis}$ due to the different Fermi surfaces we concentrate on the $s$ correction and neglect the $r$ corrections (because they have less influence on $A_{dis}$) as well as the DMR corrections, which will be small and rather similar in all three metals. We therefore employ a two-parameter description of the $\tau(k)$-dependence, using the anisotropy parameter $A_j$ and the correction parameter $s$. The results must be discussed in terms of comparisons of the known Fermi surfaces.

For an interpretation of the $s$ values in terms of the different Fermi surfaces and the different Fermi velocity distributions of the noble metals, we must look at the difference of the averaging process:

$$\tau_{Bj}^2 = \left[\left(\int_B v(k)\tau_j(k)\,dS\right)\left(\int_B v(k)\,dS\right)^{-1}\right]^2$$

and

$$s\tau_{Bj}^2 = \int_B v^2(k)\tau_j^2(k)\kappa(k)\,dS\left(\int_B v^2(k)\kappa(k)\,dS\right)^{-1}.$$

There are consequences due to the introduction of curvature, $\kappa$, as a weighting factor and due to the change from linear to quadratic averaging. We first discuss the influence of curvature on the belly: its effect is a shift of the average value $\tau$ *away* from the $\tau$ values present at the belly portions depressed below the free-electron sphere *towards* the $\tau$ values at the bulges where the curvature is appreciably stronger. Since Bragg scattering is considered to be responsible for the electron–dislocation resistivity [32] the relaxation times should be lower on the bulges than at the depressions. Thus the isolated effect of the curvature $\kappa$ as a weighting factor will be a considerable reduction of the average ($s < 1$). As the bulges (and maximum curvatures) increase slightly from silver to copper and more strongly to gold the reduction of $s$ will be slightly stronger in copper than in silver, and again only moderately stronger in gold because the higher bulges and increased curvature are confined to a smaller region.

As for the quadratic averaging $v^2\tau^2$ on its own (at constant curvature) it is shown in appendix B that the effect is an increase if the changes of $v$ and $\tau$ as a function of the position on the Fermi surface are mainly of the same sign. This is true for the characteristic $v$-dependences [28] and the relaxation times due to Bragg scattering as considered before. Moreover, for comparable $\tau(k)$-dependences this increase of $\tau(s > 1)$ grows with an increasing ratio of the highest and lowest $v$ value on the belly $r_v = v_{max}/v_{min}$.

The Fermi velocity changes on the belly are smallest for copper (18%), are increased for silver (26%) and are highest for gold (43%). The combined influence of both effects

can qualitatively explain the differences in $s$ between the noble metals. If both antagonistic effects are of similar size in gold, as is necessary for $s = 1.01$ as found there, it may be expected that for copper there will be a slightly smaller value ($s = 0.984$) as $r_v$ is strongly reduced and, as we have seen, for copper the effect of the $\kappa$-weighting factor is a moderate increase of $s$ compared with gold and simultaneously a marked decrease from quadratic averaging.

It has to be mentioned that, although the absolute values of the $s$-parameters are only inaccurately known, their differences are rather significant due to the high reproducibility of the Hall coefficient measurement. A possible shift of the DMR values due to the correction that was neglected in this treatment will also not contribute strongly, because these corrections are not too different for the metals considered. Looking at the difference $s(\mathrm{Ag}) - s(\mathrm{Cu})$ it is clear that it has to be positive, because for silver the reduction in $s$ (due to $\kappa$-weighting) is smaller than in copper and at the same time the increase in $s$ (due to quadratic averaging) is higher for silver because of its higher $r_v$. In total, this estimate shows why the TGM works well for the present case of $\tau(k)$ (electron–dislocation scattering), although the assumptions of the TGM are far from being fulfilled: the influences of squared averaging and weighting by the curvature show a strong tendency to cancel.

## 5. Conclusions

In the past, insufficient accuracy of LFHE measurements and of the calculations or estimates of the Fermi surface integrals have reduced the efficiency of the TGM. The corrected TGM explains consistently the DMR step height at 130 K and the low-field Hall coefficient of dislocated high-purity noble metals. Our investigation is consistent with isotropic electron–phonon scattering between 130–300 K. In contrast, electron–dislocation scattering is extremely anisotropic, having typical anisotropy parameters around 0.1. We may conclude that anisotropic scattering is the only important source of DMR. Although silver is the most free-electron-like noble metal, the discrepancy in averaging relaxation times between $R_H$ and DMR is largest for silver. This is due to the fact that, in the case of copper and gold, the different averaging contributions show strong cancellation.

## Acknowledgments

The author thanks M Kočer for preparing the silver samples and the DMR measurements. Further thanks are given to F Halmenschlager and M Kočer for help in automatic data acquisition. The kind support of V Gröger, B R Watts and M Müller, and their helpful discussions, are gratefully acknowledged. This work has been supported by the Fonds zur Förderung der Wissenschaftlichen Forschung under project No 9930-PHY.

## Appendix A. DMR correction

*Based on (4), the TGM and the definitions under (1), the exact total resistivity* $\rho_{tot}$ or conductivity $\sigma_{tot}$ can be written as

$$\sigma_{tot} = (1-u)\left(\sum_{j=1}^{3}\frac{1}{\tau_{Bj}}\right)^{-1}\int_B v(k)\,dS + (1-t)\left(\sum_{j=1}^{3}\frac{1}{\tau_{Nj}}\right)^{-1}\int_N v(k)\,dS$$

where

$$u = 1 - \int_B \left(\sum_{j=1}^{3} \frac{1}{\tau_j(k)}\right)^{-1} v(k)\,dS \left[\left(\sum_{j=1}^{3} \frac{1}{\tau_{Bj}(k)}\right)^{-1} \int_B v(k)\,dS\right]^{-1}$$

and

$$t = 1 - \int_N \left(\sum_{j=1}^{3} \frac{1}{\tau_j(k)}\right)^{-1} v(k)\,dS \left[\left(\sum_{j=1}^{3} \frac{1}{\tau_{Nj}(k)}\right)^{-1} \int_N v(k)\,dS\right]^{-1}.$$

The correction parameters $u$ and $t$ are defined in terms of the total resistivity of the belly and neck region within the TGM, and of the exact total resistivity of belly and neck region based on the exact averaging for each point of the Fermi surface. Using

$$\sigma_{Bj} = \sigma_j/(1 + bA_j) \qquad \sigma_{Nj} = \sigma_j bA_j/(1 + bA_j) \qquad \rho_j = 1/\sigma_j$$

we obtain approximately ($u$ and $t$ are drastically smaller than 1)

$$\rho_{tot} = \sum_{j=1}^{3}(1 + bA_j)\rho_j \sum_{j=1}^{3}(1 + bA_j)\rho_j A_{j+1}A_{j+2}\left(\sum_{j=1}^{3}(1 + bA_j)^2\rho_j A_{j+1}A_{j+2}\right)$$
$$\times\left[1 + u + (t-u)\sum_{j=1}^{3}(1+bA_j)\rho_j A_{j+1}A_{j+2}\left(\sum_{j=1}^{3}(1+bA_j)^2\rho_j A_{j+1}A_{j+2}\right)^{-1}\right]. \tag{A1}$$

As the variation of $v(k)\tau(k)$ on the belly is supposed to be lower than on the neck, but the belly portion is higher, the respective deviation parameters $t$ and $u$ will be of the same order of magnitude. Therefore, for an estimate of the DMR correction $\Delta\delta$, it seems to be appropriate to use the approximation

$$\Delta\delta = \rho_{tot}(\text{TGM})u \tag{A2}$$

where $\rho_{tot}$(TGM) is the total resistivity within the usual TGM.

## Appendix B. Estimation of quadratic averaging effects

If $\tau_{Bj}$ is inserted in $s$ (see (1)), writing a general $\tau(k)$ we obtain the following belly integrals:

$$\left[\left(\int v^2(k)\tau^2(k)\,dS\right)\left(\int v(k)\tau(k)\,dS\right)^{-2}\right]\left(\int v(k)\,dS\right)^2\left(\int v^2(k)\,dS\right)^{-1}.$$

In order to see the effect of the dominant term

$$\int v^2(k)\tau^2(k)\,dS\left(\int v(k)\tau(k)\,dS\right)^{-2}$$

the simple term $(v_1^2\tau_1^2 + v_2^2\tau_2^2)/(v_1\tau_1 + v_2\tau_2)^2$ is considered. Since only the ratio is important as can be seen from the alternative formulation

$$[(v_1^2/v_2^2) + (\tau_1^2/\tau_2^2)][(v_1/v_2) + (\tau_1/\tau_2)]^{-2}$$

we can choose (without loss of generality) $v_2 = 1$, $\tau_2 = 1$ and $v_1 > 1$. Now we find by standard discussion of the function

$$f(\tau_1) = (v_1^2\tau_1^2 + 1)(v_1\tau_1 + 1)^{-2}$$

that the function $f(\tau_1) > 1$, if $\tau_1 > 1$ or $\tau_1 < 1/v_1^2$; $f(\tau_1) < 1$, if $\tau$ is between 1 and $1/v_1^2$, with a minimum at $1/v$. For $\tau_1 > 1$ fixed, $f(\tau_1, v_1)$ increases with $v_1$.

## References


[1] Sachslehner F 1995 *J. Phys.: Condens. Matter* **6** 11 229
[2] Watts B R 1989 *Dislocations in Solids 8* ed F R N Nabarro (Amsterdam: Elsevier)
[3] Bross H and Häberlen O 1993 *J. Phys.: Condens. Matter* **5** 7687
[4] Müller M, Zehetbauer M, Sachslehner F and Gröger V 1994 *Solid State Phenomena* **35–6** 557
[5] Sachslehner F and Vodel W 1992 *Cryogenics* **32** 805
[6] Dugdale J S and Firth L D 1969 *J. Phys. C: Solid State Phys.* **2** 1272; 1969 *Phys. Kond. Mat.* **9** 54
[7] Barnard R D 1977 *J. Phys. F: Met. Phys.* **7** 673
[8] Goodarz M and Barnard R D 1977 *Phys. Status Solidi* b **83** 555
[9] Barnard R D 1980 *J. Phys. F: Met. Phys.* **10** 2251
[10] Lengeler B, Schilling W and Wenzl H 1970 *J. Low Temp. Phys.* **2** 59
[11] Sakomoto I and Yonemitso K 1987 *Japan. J. Appl. Phys.* **26** 645
[12] Zehetbauer M, Gröger V and Watts B R 1991 *Solid State Commun.* **79** 465
[13] Sachslehner F 1988 *Phys. Status Solidi* a **107** 305
[14] Gröger V 1986 *Phys. Status Solidi* a **98** 291
[15] Gröger V 1983 *Acta Phys. Austriaca* **55** 89
[16] Baratta A J and Ehrlich A C 1983 *Phys. Rev.* B **28** 4136
[17] Dugdale J S and Basinski Z S 1967 *Phys. Rev.* **157** 552
[18] Cimberle M R, Bobel G and Rizzuto C 1974 *Adv. Phys.* **23** 639
[19] Barnard R D, Alderson J E A, Farrell T and Hurd C M 1968 *Phys. Rev.* **176** 761
[20] Lengeler B, Schilling W and Wenzl H 1970 *J. Low Temp. Phys.* **2** 237
[21] Zürcher R, Müller M, Sachslehner F, Gröger V and Zehetbauer M 1995 *J. Phys.: Condens. Matter* **7** 3515
[22] Ehrlich A C 1974 *J. Mat. Sci.* **9** 1064
[23] Fickett F R 1974 *Mat. Sci. Eng.* **14** 199
[24] Matula R A 1979 *J. Phys. Chem. Ref. Data* **8** 1147
[25] Segall B 1962 *Phys. Rev.* **125** 109
[26] Halse M R 1969 *Phil. Trans. R. Soc.* A **265** 507
[27] Watts B R 1994 Private communication
[28] Lengeler B 1978 *Springer Tracts in Modern Physics 82* ed G Höhler (Berlin: Springer)
[29] Gray D E 1972 *American Institute of Physics Handbook* 3rd edn (New York: McGraw-Hill)
[30] Hurd C M 1972 *The Hall Effect in Metals and Alloys* (New York: Plenum)
[31] Watts B R 1995 to be published
[32] Watts B R 1988 *J. Phys. F: Met. Phys.* **18** 1197